PHYSICAL REVIEW E **80**, 036309 (2009)

Molecular dynamics simulations of polymeric fluids in narrow channels: Methods to enhance mixing

Srikanth Dhondi,[1] Gerald G. Pereira,[2] and Shaun C. Hendy[1]

[1]*MacDiarmid Institute for Advanced Materials and Nanotechnology, School of Chemical and Physical Sciences, Victoria University of Wellington, Wellington 6011, New Zealand*

[2]*CSIRO Mathematical & Information Sciences, Private Bag 33, Clayton South 3169, Australia*

(Received 1 June 2009; published 17 September 2009)

Mixing of shear thinning polymeric fluids in long channels with patterned boundary conditions is studied through molecular dynamics simulations. Patterned wettability was shown to induce spatially varying slip lengths at the channel walls which in turn induce mixing in the fluid. To quantify the amount of mixing for different wave lengths of patterns, transverse velocity profiles were evaluated. The transverse velocity profiles from the molecular dynamics simulations were then compared with predictions from continuum modeling and good quantitative agreement was found. Offsetting the pattern was shown to produce better mixing in the center of the channel. Transverse flow is found to increase when the radius of gyration of the chains is smaller than the pattern length. We also implement an oscillating (time dependent) body force and find that the transverse flow increases significantly. However, we do not find an increase in transverse flow with frequency of the oscillation as predicted from continuum modeling and we postulate reasons for this behavior.

DOI: 10.1103/PhysRevE.80.036309 PACS number(s): 47.57.Ng, 47.61.−k, 47.85.lk, 47.85.Np

I. INTRODUCTION

Microfluidics or nanofluidics is a rapidly developing area of physics with potential applications in chemical, biomedical and biochemical processes [1–3]. This field has attracted tremendous attention in recent years because of its capability to function with small amounts of reagents, robustness, high sensitivity, and portability to name a few [1,3]. Mixing of fluids is essential in most of the microfluidic applications [3]. Applications in the area of biochemistry, drug delivery, cell activation, protein folding etc. require rapid mixing of fluids [1]. It is well known that the flow inside microchannels is usually laminar because of the low Reynolds number associated with the flow and hence mixing is mainly diffusion dominated which is a slow process. To achieve good mixing therefore demands long channels and time scales. In general, there are two types of micromixers that are used to induce mixing in these devices, active and passive mixers. Active mixers use external perturbations such as pressure, temperature etc. [1] on the system to enhance mixing. They are rapid and externally controllable but difficult to manufacture [1]. On the other hand passive mixers use the topology of the device to promote transverse flows. These are relatively easy to manufacture but cannot be controlled externally. A good number of active and passive mixers are already in use. For a detailed study on different types of mixers the reader is referred to the article by Nguyen and Wu [1]. A good introduction to the theory behind the mixing processes can be found in the article by Ottino and Wiggins [2].

When scaling down from macroscale to microscale, fluids do not behave in the same manner as at macroscale. At microscale, different aspects come into picture such as low Reynold's number ($\mathrm{Re} \equiv \rho L v / \mu$ where ρ is the fluid's density, v is a characteristic fluid velocity, L characteristic length scale and μ is the fluid viscosity), large surface area to volume ratio (SAV) etc. Because of the large SAV, at microscale, surface properties can greatly influence the fluid flow. As pointed out earlier because of the low Re number the flow is viscous dominated therefore offers great resistance to the flow. Generally, in fluid dynamics the no-slip boundary condition is assumed at the solid-fluid interface. According to this condition the velocity of the fluid at the wall is equal to that of the wall. This boundary condition is found to be a good approximation at a macroscopic level but violations of this condition have been observed at the microscale. Recent experimental and molecular dynamics simulation studies have reported that the no-slip boundary condition at the solid-fluid interface is not obeyed in certain circumstances [4–8]. Some of these studies noticed significant slip lengths [4,5,9]. It has been demonstrated that slip at the wall-fluid boundary can be used to overcome the resistance offered in microchannels [6,10]. The slip length is defined as the distance in a direction perpendicular and into the wall where the linear extrapolation of the longitudinal component of the fluid velocity becomes zero. A detailed list of experiments and observed slip lengths is presented in the article by Lauga *et al.* [11]. However the magnitude of the slip lengths reported in some of these studies is still debated due to possible experimental errors [11]. The slip length depends on several physical properties and extensive research has been carried out in understanding the various physical properties that can influence the slippage of the fluid over the surfaces. Flow over atomistically smooth walls is shown to produce large slip lengths while an increase in the surface roughness yielded much smaller slip lengths [8,10]. Flow over chemically patterned surfaces with periodic grooves have shown formation of a composite layer at low pressures which in turn enhanced the slip lengths significantly [10]. Wettability of the surface also plays an important role in determining the slip length [8,12,13]. Using superhydrophobic surfaces slip lengths up to 2 μm were observed [4]. A strong interaction at the solid-wall interface produces a small slip length and vice versa [8]. Barrat and Bocquet [12] conducted molecular dynamics simulations of a Newtonian fluid in a nanopore.

They have noticed that changing the wettability parameter changes the slip length of the fluid at the solid-fluid interface. In this study they found that decreasing the wettability of the wall increased the slip length.

Shear dependent slip behavior of Newtonian fluids was studied by Zhu and Granick [14]. They found that slip length increases with an increase in the shear rate. A more detailed study of the relationship between the shear rate and slip length for Newtonian fluids was conducted by Thompson and Tronian [7]. In this case the slip length was found to increase with the applied shear rate up to a critical value. Shear rate dependence of slip for polymeric fluids have yielded similar results [15]. The slip length was also found to increase with the chain length up to the entanglement length.

In the context of fluid mixing, it has been suggested this slip behavior of the fluid at the wall can be used to overcome some of the limitations posed by the laminar flow. Using patterned substrates in microchannels, Kuksenok *et al.* [16] found that mixing of binary fluids can be enhanced. Poiseuille flow of binary fluids over chemically patterned patches of wettable and nonwettable regions induced transverse flows in this study. Hendy *et al.* [17] have studied the flow of Newtonian fluid over the patterned wettable walls analytically and compared the results with molecular dynamic simulations. They studied the effect of patterned wettability, by creating regions of high and low slip along the channel walls, on the fluid flow. By putting a pressure difference over the channel ends, which would normally induce a Poiseuille type flow, they observed significant transverse flows. Ou *et al.* [18] exploited this effect to create a microscale device based on hydrophobic ridges that was found to enhance mixing of an aqueous dye. However mixing of macromolecules in microfluidic devices is important in applications dealing with biomolecules or polymers [1,3]. Because of the macromolecular nature of such fluids, diffusion can be a much slower process than for simple fluids which is undesirable in many practical applications. Thus, methods for rapid interspersion of polymeric fluids need to be considered. Pereira [19] has carried out a perturbation analysis of a continuum theory for a visco-elastic fluid with patterned slip boundary conditions along the lines of Hendy's [17] work. From this study he found that mixing is enhanced for shear thickening fluids but suppressed for shear thinning fluids, when compared to Newtonian fluids. Furthermore, applying a time dependent pressure it was shown that transverse flows were enhanced for elastic fluids.

In this paper, we discuss the implementation of molecular dynamic simulations of polymeric fluids over the patterned wettable surfaces and study their mixing behavior. The paper is organized in the following way. In Sec. II we give details on the simulation method, in Sec. III we characterize the nature of the fluid and its continuum characteristics by carrying out Couette and Poiseuille flow simulations while in Sec. IV we study the flow of these fluids over patterned surfaces and compare the results with continuum models.

II. SIMULATION METHOD

The simulation domain consists of a coarse grained bead-spring polymeric fluid confined between two atomistically flat walls. The simulation geometry is shown in Fig. 1 with the walls lying in the *xz* plane and flow occurring in the *x* direction. Each wall contains up to three deep fcc (100) atom layers. Throughout all the simulations the wall atoms were fixed in space and there was no interaction between them. The interaction between the wall atoms and fluid monomers and between the nonbonded fluid-fluid monomers was modeled by the shifted Lennard-Jones (LJ) potential given by

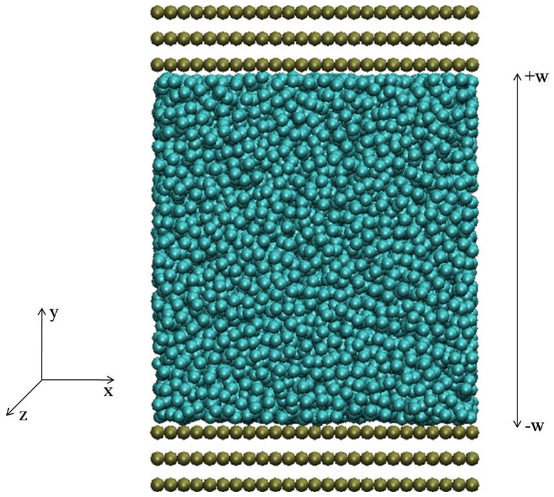

FIG. 1. (Color online) *xy*-cross section of the simulation setup is shown here. The volume between the two parallel plates, placed at $\mp w$, was filled with polymeric fluid.

$$\Phi_{LJ}(r)=\begin{cases}4\varepsilon\left[\left(\frac{\sigma}{r}\right)^{12}-\left(\frac{\sigma}{r}\right)^{6}-\left(\frac{\sigma}{r_c}\right)^{12}+\left(\frac{\sigma}{r_c}\right)^{6}\right] & \text{if } r\le r_c\\ 0 & \text{if } r>r_c\end{cases}$$

with a cutoff radius of $r_c=2.5\sigma$ unless otherwise specified. Here r is the distance between the particles, while ε and σ are the energy and length scales used in the simulation. The density of the wall ρ_w was fixed at 0.7 σ^{-3}. Wall-fluid and fluid-fluid energy parameters are represented by ε_{wf} and ε_{ff}, respectively. The nonbonded monomers interact via the LJ potential with $\varepsilon_{ff}=1.0$. This parameter for the nonbonded monomer-monomer interaction was constant throughout all simulations discussed in this paper. In addition, the bonded monomers of a molecule interact via the finite extensible nonlinear elastic (FENE) potential

$$\Phi_{\mathrm{FENE}}(r)=\begin{cases}-\frac{1}{2}kr_0^2\ln[1-(r/r_0)^2] & \text{if } r\le r_0\\ \infty & \text{if } r>r_0\end{cases}$$

where parameters $r_0=1.5\sigma$ and $k=30\varepsilon\sigma^{-2}$ [20]. This set of parameters ensures that there are no bond breakages or chain crossings. In all our simulations we have used $\sigma=1.0$. The density of the fluid was maintained at $\rho\approx0.9\sigma^{-3}$ with each polymer chain consisting of $N=20$ monomers. The mass of both the fluid monomers and wall atoms was set to 1.0. The temperature of the system was controlled by thermostating the fluid monomers using the Langevin thermostat. To avoid interference with the flow direction only the z component of the equation of motion was thermostated [21]. The temperature of the fluid was maintained at $T=1.0\varepsilon/k_B$. The governing equations of motion are

$$m\ddot{x}_i = -\sum_{i\neq j} \frac{\partial \Phi_{ij}}{\partial x_i}, \tag{1}$$

$$m\ddot{y}_i = -\sum_{i\neq j} \frac{\partial \Phi_{ij}}{\partial y_i}, \tag{2}$$

$$m\ddot{z}_i + m\Gamma\dot{z}_i = -\sum_{i\neq j} \frac{\partial \Phi_{ij}}{\partial z_i} + f_i, \tag{3}$$

where $\Gamma=1.0\tau^{-1}$ is the friction constant and f_i is the random force acting on particle i that mimics the random collisions taking place between the fluid particles. Here $\tau=\sqrt{m\sigma^2/\varepsilon}$ is the characteristic LJ time scale. Periodic boundary conditions were applied in x and z directions. The equations of motion were integrated using the Verlet algorithm [22]. The time step size used in our simulations was $\Delta t=0.001\tau$. All the quantities are expressed in reduced LJ units.

The initial configuration of the fluid was generated by randomly placing polymer chains in the given volume. Because of the random placement of the polymer chains, the initial configuration is highly overlapping and using the LJ potential between the fluid monomers would lead to unphysical results such as bond breakings. Therefore we must use a mechanism by which the initial melt is uniformly distributed in space without any overlaps. To do this we use the soft potential between the fluid monomers [23],

$$\Phi_s(r) = \begin{cases} A[1+\cos(\pi r/r_c)] & \text{if } r \le r_c \\ 0 & \text{if } r > r_c, \end{cases}$$

where the prefactor A is the amplitude of the interaction energy and $r_c=1.1226\sigma$ is the cutoff radius. The system was equilibrated for 50τ using this potential. The value of A increases in time from 0.0 to 60.0 during this period. After this time period we achieved a reasonably uniform melt and the interaction between monomers can now be changed to the LJ potential. The system was further equilibrated using the LJ potential first for 50τ with $r_{c_{ff}}=1.12246\sigma$ then for another 50τ with $r_{c_{ff}}=2.5\sigma$. After this equilibration period the cutoff radius was fixed at $r_{cff}=2.5\sigma$ for the rest of the simulation. Here $r_{c_{ff}}$ denotes the cutoff radius for the interaction between the fluid-fluid monomers. The above procedure was the first step in all the simulations mentioned in this paper.

III. CHARACTERIZATION OF POLYMERIC FLUID

We now begin our discussion of the MD simulations. The first thing we need to do is fully characterize the polymer melt that we simulate and relate it to the continuum model [19]. Once this is established we can proceed to carry out the simulations with variable boundary conditions and variable pressure gradients.

A. Couette flow

Initially, a set of Couette-flow simulations were carried out to determine the nature of the fluid, that is whether the fluid is shear thinning or shear thickening. To begin with both walls were fixed and the fluid was equilibrated using the method described in the last section. Then, the upper wall was slowly moved in the x direction while the lower wall was stationary. The LJ interaction energy between the wall atoms and monomers was set to $\varepsilon_{wf}=1.0$. To realize the physical situation the velocity of the upper wall was increased in steps of $0.1\sigma\tau^{-1}$ starting from zero up to U, the desired velocity at which the upper wall moves. After each velocity increment, the system was equilibrated for 10τ, until it reached the final velocity U. When the upper wall velocity reached the desired value U, a further equilibration was done for 500τ to achieve steady state. The average velocity profiles were calculated by dividing the system in the y direction into bins of size $\Delta y=0.2\sigma$. At each time step the fluid particles were mapped into one of these bins and the average velocity in those particular bins was calculated. A time average of $u_x(y)$ was obtained over the next $10^3\tau$. A number of simulations with different wall velocities (shear rates) were conducted and the corresponding velocity profiles are shown in Fig. 2. We have observed that the slip length is dependent on the applied shear rate and this is consistent with the literature [15,24,25]. The shear rate is defined as $\dot{\gamma}=U/2w$, where $2w$ is the separation between the walls. An increase in the slip length was observed with an increase in the shear rate. The slip length as a function of shear rate is shown in Fig. 3. This result is in agreement with the previous polymer flow studies where the slip length of the polymeric fluid in Couette flow simulations was found to be dependent on the applied shear rate [24,25]. We find general qualitative agreement with these previous studies, although direct quantitative comparison is not possible since they were conducted under different conditions which affect the measured slip length. A slight curvature was observed in all velocity profiles at a distance approximately σ away from both walls and this deviation from linearity close to the walls can be attributed to layering of fluid particles that takes place near the walls. The stress tensor components were calculated by the Irving-

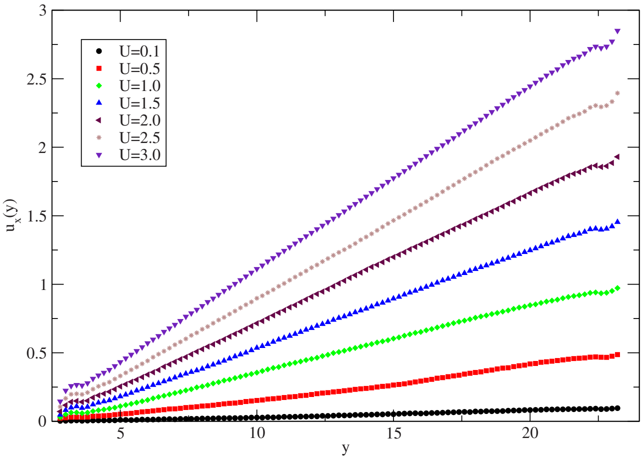

FIG. 2. (Color online) Longitudinal velocity profiles obtained for different upper wall velocities U. The velocity profiles are linear except for slight curvature up to a distance of σ away from both inner wall surfaces. The magnitude of the velocity profiles is linear in U.

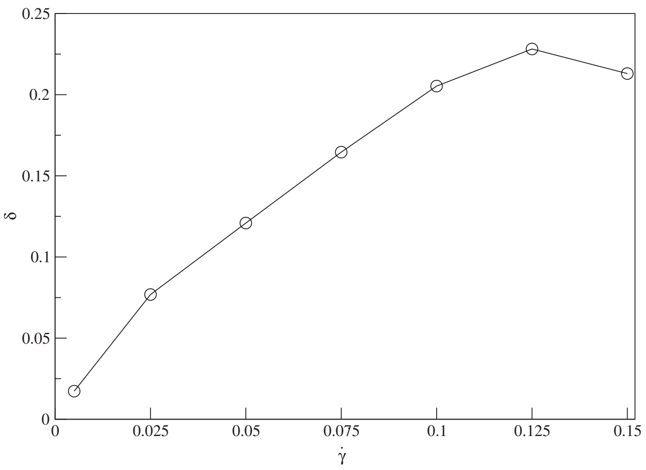

FIG. 3. The slip length is calculated for different shear rates. It increases almost linearly before starting to decrease.

Kirkwood method [26]. We used an atomistic description of this model as mentioned by Jabbarzadeh *et al.* [27],

$$\sigma_{xy} = -\frac{1}{V}\left\langle \sum_{i=1}^{N} m_i u_{ix} u_{iy} + \sum_{i=1}^{N}\sum_{j>i}^{N} \mathbf{r}_{ijx}\mathbf{F}_{ijy} \right\rangle, \tag{4}$$

where V is the volume of the system. The first term in the above equation is the kinetic energy contribution to the stress tensor and u_{ix} and u_{iy} are the velocity components of the particle i in x and y directions, respectively. The second term is the potential energy contribution from the pair wise and bond interactions where $\mathbf{r}_{ijx}$ is the x component of the distance vector between particles i and j and $\mathbf{F}_{ijy}$ is the force component in the y direction between particle i and j. The shear viscosity is defined as

$$\eta = \frac{\sigma_{xy}}{\dot{\gamma}}. \tag{5}$$

We have used the power law model to calculate the viscosity of the fluid. The viscosity of a power law fluid [28] is given by $\eta = m(\dot{\gamma})^{n-1}$, here m is the consistency coefficient and the exponent n determines the nature of the fluid. A value of $n<1$ means the fluid is shear thinning and $n>1$ corresponds to a shear thickening fluid. Fig. 4 shows the fluid viscosity η as function of increasing shear rate $\dot{\gamma}$. Large error bars were noticed at low shear rates and the magnitude of the error bars diminished with an increase in the shear rate. This is because at low shear rates the thermal velocity of the fluid is greater than the velocity of the fluid itself thus leading to large error bars in viscosity [25,29,30] at low shear rates. By measuring the gradient of the curve in Fig. 4, for large shear rates, we found $n = 0.607\,63 \pm 0.0138\,71$ suggesting that the fluid under consideration is shear thinning. The value of the consistency coefficient m was found to be 1.839 92.

B. Determining the slip length

The slip length of the fluid at the wall-fluid interface is strongly influenced by the interaction between them. To study and quantify the effect of the wall-fluid interaction energy ε_{wf} on the slip length δ, Poiseuille-type flows were simulated by applying a constant body force on each monomer in the x direction. A body force of $F = 0.05m\sigma/\tau^2$ was applied on each fluid particle at every time step while the wall atoms remained stationary. The fluid was driven through the channel by the body force, in the absence of a pressure gradient, this effectively gives rise to a Poiseuille type flow [31,32]. For a particular value of ε_{wf} the fluid was initially equilibrated for $1.5\times10^2\tau$. Then the body force was applied on the system gradually in steps of $0.01m\sigma/\tau^2$ until it reached the desired value of $0.05m\sigma/\tau^2$. At each increment of body force the system was allowed to equilibrate for 10τ. Once the body force reached $F = 0.05m\sigma/\tau^2$, the system was equilibrated for a further $10^3\tau$ to attain steady state. After the equilibration period, average longitudinal velocity profiles were calculated by dividing the fluid particles into bins of width $\Delta y = 0.2\sigma$ in the y direction and taking averages over the next $2\times10^3\tau$. These longitudinal velocity profiles for different values of ε_{wf} are shown in Fig. 5. Once we have obtained these velocity profiles we need to calculate the slip lengths. Our simulation results can be fit to the theoretical predictions and by doing so we can extract the slip lengths. To calculate slip lengths we need to solve the Navier-Stokes equations,

$$\rho\left(\frac{\partial \mathbf{u}}{\partial t} + \mathbf{u}\cdot\nabla\mathbf{u}\right) = -\nabla\cdot\underline{\underline{\Pi}} + \rho\mathbf{F}, \tag{6}$$

$$\nabla\cdot\mathbf{u} = 0, \tag{7}$$

where $\underline{\underline{\Pi}}$ is the stress tensor. The Navier-Stokes solution is two dimensional (x,y) since the MD simulation domain is periodic in the z direction. The left-hand side of the above Eq. (6) is assumed to be zero since the flow is considered to be laminar. Furthermore, we must have $u_x = u_x(y)$ since we have $u_y = 0$ from Eq. (7). We use the Navier slip-boundary condition to solve the Navier-Stokes equations. According to the Navier slip-boundary condition the longitudinal velocity

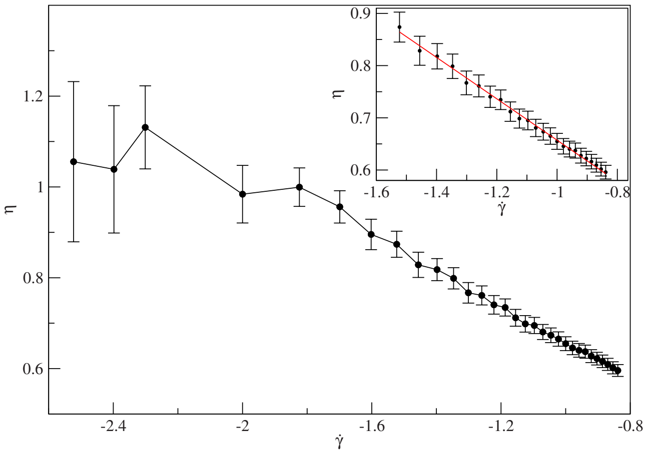

FIG. 4. (Color online) Log-log plot between shear viscosity η and shear rate $\dot{\gamma}$. The viscosity of the fluid is given by $\eta = m(\dot{\gamma})^{n-1}$. At high shear rates the plot is linear and can be seen in the embedded figure. A linear fit at high shear rates using the above equation yields a value of $n = 0.607\,63 \pm 0.013\,871$.

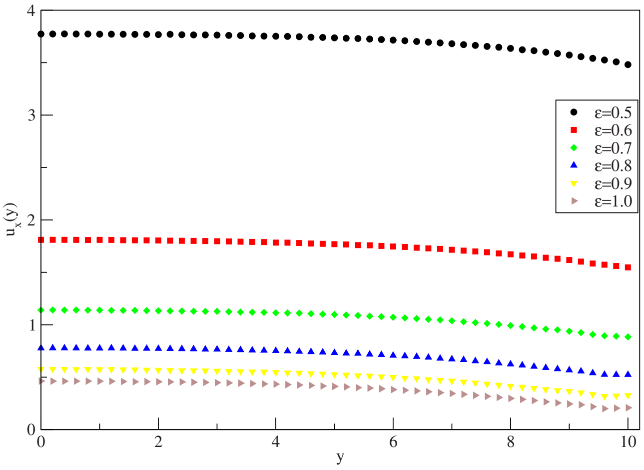

FIG. 5. (Color online) Average longitudinal velocity profiles from simulations for different values of ε_{wf} for $y \geq 0$. Note, the longitudinal velocity profile is symmetric about $y=0$.

component of the fluid at the solid wall is not zero but given by

$$u_x(\pm w) = \mp \delta \frac{\partial u_x}{\partial y}(\pm w), \tag{8}$$

where δ is the slip length. Thus solving Eq. (6) appropriately yields the resulting longitudinal velocity profile

$$u_x(y) = \left(\frac{Fw\rho}{m}\right)^{1/n}\left[\frac{w}{1+1/n}\left\{1-\left(\frac{y}{w}\right)^{1+1/n}\right\}+\delta\right]$$

$$\text{for } \; y \geq 0, \tag{9}$$

where m and n can be obtained from the Couette flow simulations. Note that $u_x(y)$ is symmetric about $y=0$. Thus all the symbols in Eq. (9) are known except for the slip length δ. By fitting Eq. (9) to the velocity profiles in Fig. 5 we obtain the relationship between ε_{wf} and δ. The effect of interaction parameter ε_{wf} on the slip length δ is shown in Fig. 6. The slip length was found to decrease with increasing ε_{wf}. This is physically realistic since a larger ε_{wf} implies that monomers will be attracted to the wall and consequently will tend to stick to it, leading to a small slip length δ.

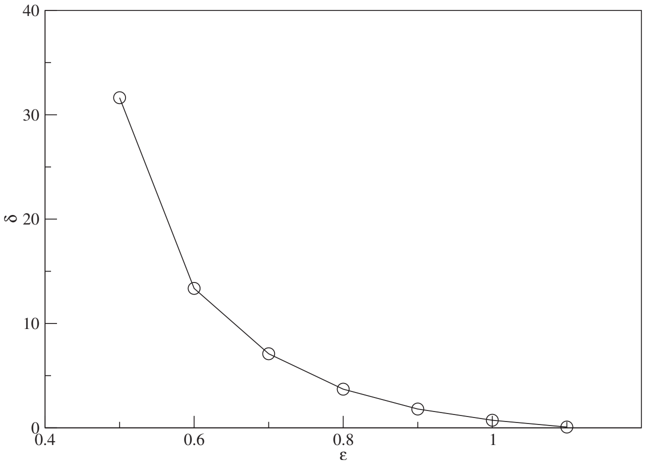

FIG. 6. Slip length δ as a function of the interaction parameter ε_{wf}.

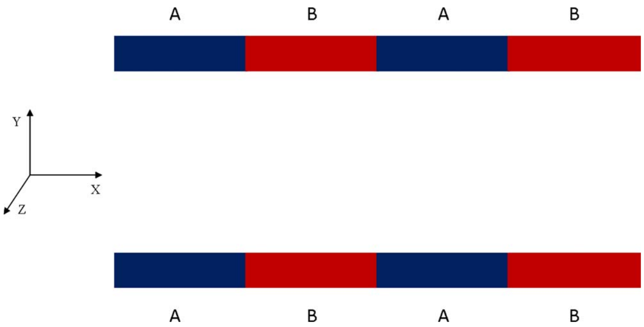

FIG. 7. (Color online) Schematic diagram representing the pattern slip boundary condition.

IV. MD SIMULATIONS FOR ENHANCED MIXING

A. Patterned boundaries

We now address the important part of our work, which is studying the effect of the patterned slip boundary condition on the fluid flow. The patterned slip boundary conditions were implemented by creating alternate regions of high slip (low wettability) and low slip (high wettability) along the walls in the x direction. As discussed in the earlier section this can be done by varying the wall-fluid interaction parameter ε_{wf}. In our simulations, this was done by creating two types of the wall atoms, A and B. If the fluid interacts with A-type wall atoms then the LJ interaction parameter is $\varepsilon_{wf_1}=0.5$ and the interaction parameter is $\varepsilon_{wf_2}=0.9$ if the fluid interacts with the B-type wall atoms. Consequently fluid particles experience a large slip when they interact with wall atoms of type A and a small slip when they interact with wall atoms of type B. This setup is shown in Fig. 7.

The system was brought to equilibrium using a similar approach to that discussed in the previous section. After the equilibration period, at each time step the y-velocity component $u_y(x,y)$ of the monomers was binned into regions of area $\Delta x \Delta y = 1.0\sigma^2$. Transverse velocity profiles were evaluated by averaging the particle $u_y(x,y)$ into one of these bins over the next $4 \times 10^3 \tau$. This averaging period was found to be sufficiently large as results obtained with longer averaging periods have shown no significant deviations.

We have carried out simulations with different pattern wave lengths. The wavelength λ (or wave number $k = 2\pi/\lambda$) of the pattern can be varied by changing the length of A or B type wall atom regions. Simulations were conducted with different pattern lengths i.e., different kw values (where w is half width of the channel), and their effect on the transverse velocity was quantified. The obtained time-averaged transverse velocity profiles for $kw = \pi/2$, $2\pi/3$, π, $4\pi/3$, and 2π are shown in Fig. 8. Alternate circular regions of high positive and negative transverse velocities were observed in the both upper and lower halves of the xy-cross section about the channel axis. The transverse velocity is close to zero along the center of the tube and near the walls with a maximum in

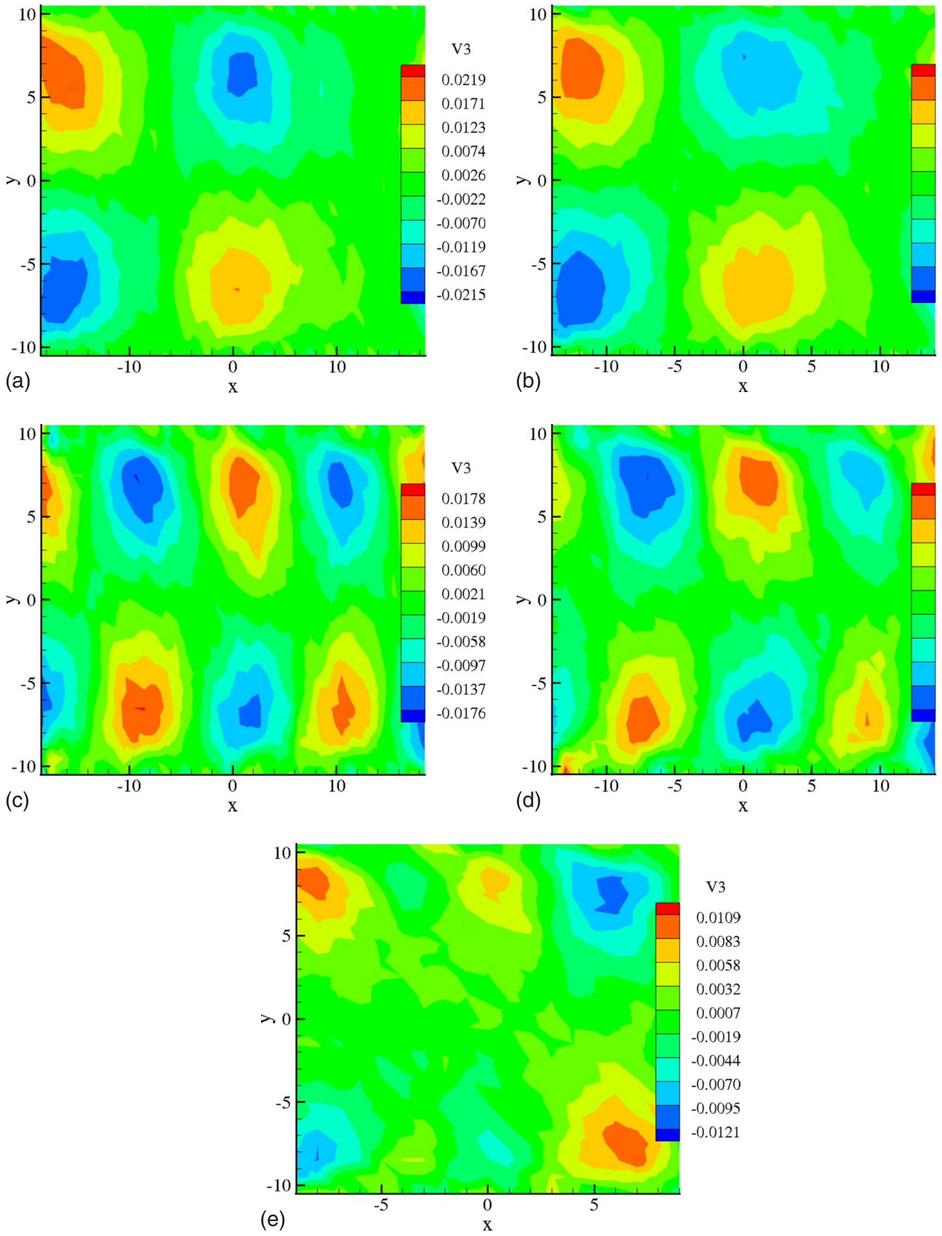

FIG. 8. (Color online) Contour plots of the transverse velocity profile $u_y(x,y)$ for various kw. Alternative high positive or negative transverse velocity regions (dark) were observed in both upper and lower halves of the channel.

between. The transverse velocity profiles are antisymmetric about the center of the channel. Thus if the upper half has a positive transverse velocity region then the lower half has a negative transverse velocity region. This creates fluid flow in the transverse direction in such a way that good mixing is achieved. However, we have observed that these transverse velocity regions do not exactly align with the wall pattern. This observation is consistent with continuum theory which suggests that there is a phase lag of $\pi/2$ between the actual pattern and the transverse velocity response [17,19]. The vorticity defined as $\mathbf{\Omega} \equiv \nabla \times \mathbf{u}$, corresponding to the case where $kw = \pi/2$ is shown in Fig. 9. (Note, the dominant Pouseille velocity has been subtracted from $\mathbf{u}$ to obtain this plot.) The vorticity is (approximately) symmetric about the x axis. Consider the domain $x > 0$. In this domain the maximum magnitude of the vorticity occurs in the region between the maximum magnitude of the transverse velocity. This is in agreement with the expectations from continuum theory [19]. Along the axis of the channel the vorticity is small as in these regions the flow is predominantly in the longitudinal direction.

To get a clear picture of what was happening on the molecular levels we have taken few snapshots of two polymer chains at different times (Fig. 10). The figure clearly shows that the polymer molecules change their positions in the transverse direction. The polymer molecules were also found to change their conformations as opposed to stretch in the direction of the flow as reported in previous studies [15]. This might be a direct consequence of using periodic wettable and nonwettable regions. The polymer molecules would like to wet the surface in some regions therefore prefer a more closely bound conformations whereas in the non-

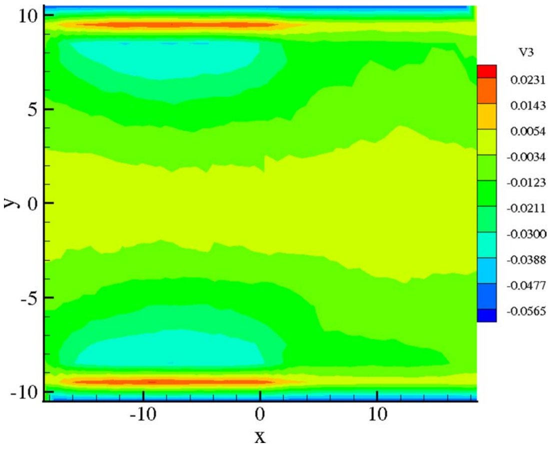

FIG. 9. (Color online) The vorticity calculated for the same simulation as Fig. 8(a). Note, maximum vorticity occurs in the region between maximum magnitude of transverse velocity.

wettable regions they would like to get away from the walls and hence take up more elongated conformations.

Well developed transverse flows were observed when the radius of gyration of polymers (R_g) is smaller than the pattern length. The average radius of gyration of the polymer chains used in our Poiseuille flow simulations under constant slip boundary condition (ε_{wf}=1.0) was R_g=5.369σ. However, in the case of kw=2π the pattern length was 4.8σ which is less than the radius of gyration of the polymers. In this case the transverse flows were suppressed. The ratio of the length of the patterned region to the radius of gyration of polymer chains seems to be an important factor in determining the amount of transverse flow that can be achieved. When the length of a patterned region is comparable with the radius of gyration of the polymer chains then, on average, a polymer chain spans two different wettable wall regions simultaneously. Hence these chains start interacting with the wall as if it is a homogeneous continuum and thus decreasing the transverse flow. In our simulations for kw=2π, the length of a patterned region was less than the radius of gyration of polymer chains and we have noticed a significant drop in the transverse velocity. The magnitude of the maximum transverse velocity in this case decreased by a factor of 2 compared to the magnitude of the maximum transverse velocity for kw=π/2. We have also observed that the transverse flow was not as well developed as in the other cases where the R_g was less than the pattern length. This indicates that the length of the patterned regions should be longer than radius of gyration to enhance transverse flows. This is an important result, which is not captured by the continuum modeling since it does not contain information about individual chains and hence does not include the length-scale R_g. Alternatively, putting these two results together leads us to a relationship between channel width and radius of gyration for maximum transverse velocity, i.e. $w > R_g/2$. Of course, the upper limit on the channel width is given by (external) physical restrictions.

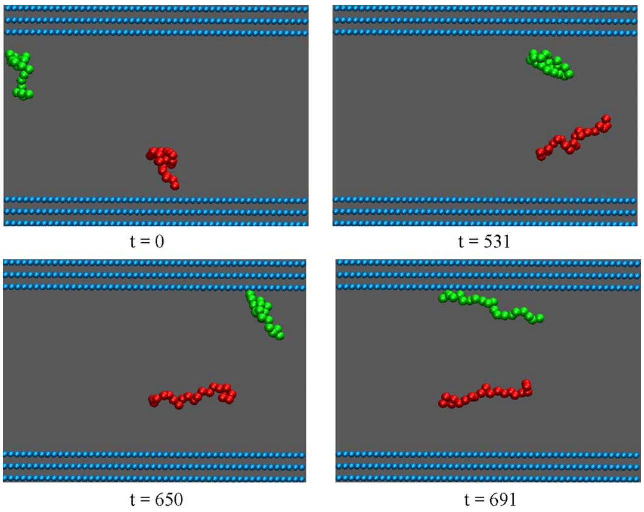
t = 0
t = 531
t = 650
t = 691

FIG. 10. (Color online) Snapshots of polymer conformations at different times. Note, on average chains near the middle of the channel are more elongated in the x direction compared to chains near the boundaries. In addition, chains near the boundary are more compact.

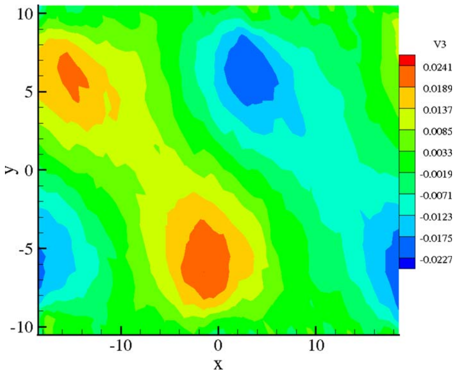

FIG. 11. (Color online) Contour plot of transverse velocity profile $u_y(x,y)$ for kw=π/2 with offset patterning.

Simulations with offset patterning of the walls were also conducted to study their effect on the transverse flow. The offsetting was done by moving the upper wall patterning by 3.2σ to the right and keeping the lower wall's position unchanged. We refer to the earlier case where the patterns were exactly parallel to each other as *parallel patterning*. Results of the simulations with offsetting in the pattern have shown no significant deviations in the magnitude of the maximum transverse velocity compared to that of parallel patterning. However, the transverse velocity regions in the upper and lower halves of the cross-section do not align parallel to each other as in the case of parallel patterning but they are offset (see Fig. 11). This was expected since the offsetting in the patterning leads to different flow behavior on the either side of the channel axis and hence offsetting of transverse flow regions occurs. An interesting observation from these simulations is that the transverse velocity is nonzero, in certain regions, at the center of the channel. Hence, with this patterning setup fluid elements in the center of the channel can flow toward the boundaries. In contrast, in the parallel patterning case, the transverse fluid velocity in the center of the channel is always zero and thus these fluid elements would never mix (except through diffusion). Therefore we suggest to obtain mixing throughout the channel, it is better to have offset patterned regions on opposite sides of the channel.

B. Comparison with continuum modeling

We would like to compare our results with the continuum modeling [19] which was based on a perturbation analysis and valid only for small variations in the slip length. In the continuum modeling the Navier-Stokes equations were solved using the Navier slip boundary condition. The patterned slip boundary condition was implemented by defining the slip length as a function of x,

$$\delta = \delta_0(1 + \alpha e^{ikx}), \tag{10}$$

where α is small perturbation about the mean value of slip length δ_0. Because of the variation in the slip boundary conditions both u_x and u_y must be functions of x and y. Using the perturbation analysis the longitudinal and transverse velocity profiles can be written as

$$u_x = u_{x_0} + \alpha u_{x_1} + O(\alpha^2) + \cdots, \tag{11}$$

$$u_y = \alpha u_{y_1} + \cdots, \tag{12}$$

where u_{x_0} is given by Eq. (9). Thus solving the Navier-Stokes equations with the above conditions yields

$$|u_y| = \alpha \psi R, \tag{13}$$

where

$$\psi = w\left(\frac{Fw\rho}{m}\right)^{1/n} \tag{14}$$

and R is given by the solution of the following differential equation

$$\begin{aligned}\bar{y}^2\frac{d^4R}{d\bar{y}^4} &+ 2(1-1/n)\frac{d^3R}{d\bar{y}^3}\\ &+ 2[\bar{y}^2(kw)^2(1-2/n) - (1-1/n)/n]\frac{d^2R}{d\bar{y}^2}\\ &+ 2(1-1/n)(1-2/n)(kw)^2\frac{dR}{d\bar{y}}\\ &+ (kw)^2[(kw)^2\bar{y}^2 - (1-1/n)/n]R = 0,\end{aligned} \tag{15}$$

where $\bar{y} = y/w$. The boundary conditions for the above equation are

$$R(0) = 0, \tag{16}$$

$$R(1) = 0, \tag{17}$$

$$R''(0) = 0, \tag{18}$$

$$R'(1) + (\delta/w)R''(1) = (\delta/w)(kw). \tag{19}$$

To attain a reasonable comparison between the continuum analysis and molecular dynamics simulations, we carried out simulations corresponding to a small α. Looking at Fig. 6 the optimal ε_{wf} values were found to be $\varepsilon_{wf_1}=0.8$ and $\varepsilon_{wf_2}=0.9$ for $kw=\pi$. In this case, the maximum transverse velocity produced in the MD simulation was $u_{y_{\max}}=0.007$. (Note, for the MD simulations, patterning of the boundaries is carried out as described in Secs. III B and IV A, so that we have a square-wave variation in the slip length. While continuum theory assumes a sinusoidal variation in the slip length we have found from our previous work [17] that the transverse flows are quite similar in both cases, as long as α is sufficiently small.) In order to compare this molecular dynamics result with the continuum analysis we need to obtain an α value from our simulation. An estimate of α was obtained using the following method. The slip lengths are $\delta_1/w=0.363\,133$ and $\delta_2/w=0.176\,313$ for $\varepsilon_{wf_1}=0.8$ and $\varepsilon_{wf_2}=0.9$, respectively, corresponding to a mean value of $\delta_0/w=0.2697$. Thus we define α by

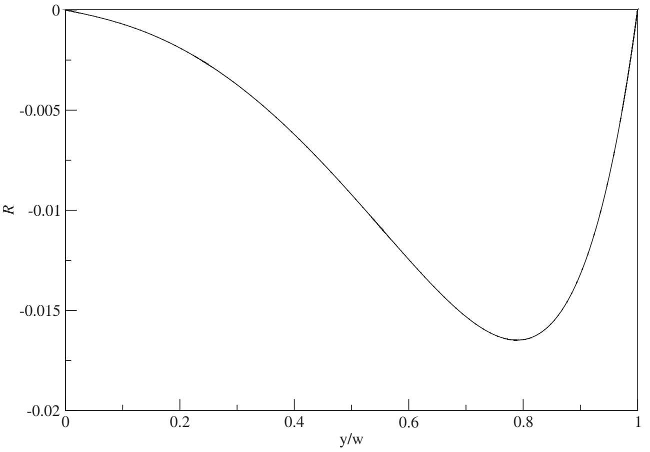

FIG. 12. The function R as a function of y/w solved using Eq. (15) with parameters selected to agree with molecular dynamics simulation (see text).

$$\delta_1 = \delta_0(1 + \alpha), \tag{20}$$

$$\delta_2 = \delta_0(1 - \alpha). \tag{21}$$

Solving for α from the above two equations yields $\alpha=0.3463$. Although we could have used another set of interaction parameters to get a much smaller value of α, we have observed that this leads to a very small transverse flow which is difficult to distinguish from pure thermal motion. Thus we use this value of $\alpha=0.3463$ to make a comparison between the continuum theory and simulations. The continuum equations were solved using these set of parameters numerically and the result is shown in Fig. 12. Thus using Eqs. (13) and (14) together with the value of α given above and the maximum magnitude from Fig. 12 we find a maximum transverse velocity $u_{y_{\max}}=0.0058$. Thus, the maximum value of the transverse velocity obtained from the theory and molecular dynamics simulations compare quite well.

C. Time dependent body force coupled to patterned boundaries

It has been shown by Pereira [19] that the transverse flow for shear thinning fluids can be enhanced by coupling a time dependent pressure gradient with patterned slip boundary condition. In our case this can be achieved by applying a sinusoidal body force as a function of time. We will briefly discuss the theory involved. The sinusoidal body force applied on each monomer is given by

$$F = F_0[1 + \epsilon \sin(\omega t)], \tag{22}$$

where the body force F fluctuates about the mean body force F_0 with a small perturbation ϵ and ω is the frequency of the oscillation.

The fluid behavior was modeled by a linearized White-Metzner model. According to this model

$$\underline{\underline{\tau}} + \Lambda \frac{\partial \underline{\underline{\tau}}}{\partial t} = - \eta(\dot{\gamma}) \underline{\underline{\dot{\gamma}}}, \tag{23}$$

where Λ is the relaxation time of the fluid. The longitudinal and transverse velocity profiles can be obtained by using the perturbative approach by expanding the velocity profiles in terms of α and ϵ.

$$u = u_0 + \alpha u_1 + \epsilon[u_{10} + u_{11} \sin(\omega t)] + \alpha\epsilon[u_{\alpha 10} + u_{\alpha 11} \sin(\omega t)] + O(\alpha^2, \epsilon^2) + \cdots \tag{24}$$

$$v = \alpha v_1 + \alpha\epsilon[v_{\alpha 10} + v_{\alpha 11} \sin(\omega t)] + \cdots \tag{25}$$

The sinusoidal body force effect on the transverse flow can be quantified by solving $v_{\alpha 11}$ [19]. Solving the Navier-Stokes equations using the above equations with appropriate boundary conditions yields

$$|v_{\alpha 11}| \propto (1 + \Lambda^2 \omega^2)^{1/2}. \tag{26}$$

Thus the model predicts a sinusoidal body force should increase the magnitude of the transverse flow and, furthermore, this magnitude increases with increasing frequency of the oscillating body force. The above model was necessarily simplified since it was required to obtain semianalytic solutions or, at the very most, numerical solutions which were not too complex. We will discuss some of the deficiencies in this continuum modeling below especially in relationship to our MD simulations.

We apply a sinusoidal body force with a perturbation constant, ϵ, in Eq. (22) set to 0.1, so that the maximum value of this oscillating body force was 10% larger than for the constant case. The frequency ω was increased from $2\pi/100$ rads/τ to $2\pi/10$ rads/τ. The body force was changed incrementally after every τ time to allow the thermostat to stabilize the temperature of the system. In each of these simulations the system was equilibrated roughly for $2 \times 10^3 \tau$. The first thing we require to do is to verify that our fluid behaves like an elastic fluid. Thus when we apply a sinusoidal body force we expect that an elastic fluid will also respond with a sinusoidal longitudinal velocity. However, because of viscous dissipation, the fluid will be out of phase with the body force. According to the continuum model of Pereira [19] the phase angle, ϕ that the longitudinal velocity lags behind the body force is related to Λ and the forcing frequency, ω by

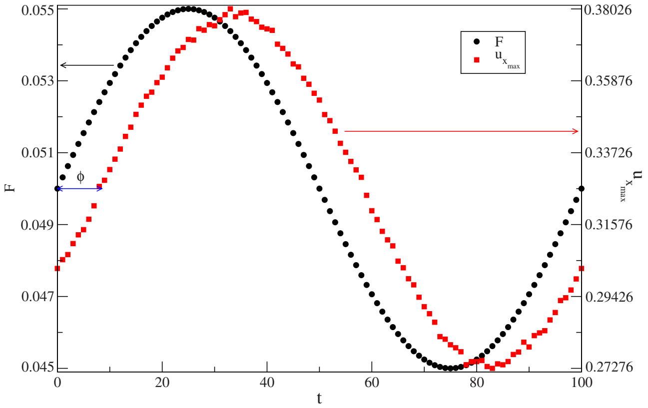

FIG. 13. (Color online) The body force (circles) and maximum longitudinal velocity response (squares) as a function of time. The scale on the left-hand side represents body force and the one on the right-hand side represents the magnitude of $u_{x_{max}}$.

$$\phi \equiv \arctan(\Lambda\omega). \tag{27}$$

Simulations were initially carried out at frequencies $2\pi/100$, $2\pi/40$, $2\pi/30$, $2\pi/20$, and $2\pi/10$ rads/τ and with homogeneous slip boundary conditions, i.e., boundaries were not patterned. Note, we cannot increase the frequency of the sinusoidal body force to too large a value since the polymer chains will not have sufficient time to respond to changes in body force.

In response to the sinusoidally varying body force, we expect a sinusoidally varying Poiseuille flow in the channel. In each case we found that the response of the fluid was indeed sinusoidally time varying so that the fluid is indeed elastic. In addition, the longitudinal velocity lagged behind the body force. For example, the body force and the longitudinal velocity response are shown in Fig. 13 for the case where $\omega = 2\pi/100$ rads/τ. Note, the longitudinal velocity shown was an average over 1000 configurations, where the averaging was done every $T\tau$, where time period $T = 10, 20, 30, 40, 100$ depending on the particular frequency being studied. The phase lag is marked in Fig. 13. To obtain a precise value of this phase lag we fit the longitudinal velocity data (circles) to a sinusoid, i.e., $A \sin(\omega t + \phi) + A_0$. A_0 and A can be obtained from the data while ω is known. We carry out a least squares fit to obtain ϕ. In each case the least squares error was found to be less than 10^{-3}. The phase lags calculated according to this method are given in Table I. As the forcing frequency increases we find the phase lag correspondingly increases, which is expected since for higher frequencies the polymer chains cannot respond sufficiently quickly, leading to a larger phase lag. The largest phase lag that can occur is $\pi/2$ rads. Now, according to Eq. (27) we can also obtain Λ for the polymer melt. These are also tabulated in Table I. Interestingly, for each forcing frequency we find a different Λ, with the Λ's systematically increasing with frequency. Thus we see an important deficiency of the simplified continuum model [19]—it employs only a single relaxation constant, Λ. As pointed out above this simplification was used to obtain tractable solutions. However, a better model for our viscoelastic fluid would be a *Generalized lin-*

TABLE I. Phase lag (ϕ), relaxation time (Λ), maximum of transverse velocity ($u_{y_{\max}}$) and percentage increase in maximum transverse velocity compared to constant body force case for various sinusoidally varying body force frequencies.

ω	$2\pi/100$	$2\pi/40$	$2\pi/30$	$2\pi/20$	$2\pi/10$
ϕ	0.516	1.007	1.167	1.375	1.571
Λ	9.02	10.08	11.17	16.08	∞
$u_{y_{\max}}$	0.0287	0.0284	0.0283	0.0281	0.0288
% increase	21.2	20.1	19.7	18.8	21.7

ear viscoelastic model [28], that is a superposition of linear White-Metzner models of the form

$$\underline{\underline{\tau}}(t)=\sum_{k=1}^{\infty}\underline{\underline{\tau}}_k(t);\qquad \underline{\underline{\tau}}_k+\Lambda_k\frac{\partial\underline{\underline{\tau}}_k}{\partial t}=-\eta_k(\dot{\gamma})\underline{\underline{\dot{\gamma}}}. \tag{28}$$

Given that there is not a single Λ that describes our fluid, but in principle an infinite number of them we might not expect the response of the fluid to be exactly as specified by Eq. (26).

We now proceed to discuss the simulations with the (same) patterned boundary conditions as discussed in the earlier section but in conjunction with the sinusoidal body force. Now the transverse velocity profile changes with the body force which is a sinusoidal function of time. To calculate average transverse velocity profiles we have to consider only those profiles which are separated by $T\tau$. We take 5000 such configurations to evaluate the transverse velocity profiles for each frequency which was found to be a sufficient number of averages to compare with the constant body force case. Note, to carry out these 5000 averages for the simulation with forcing frequency of $2\pi/100$ took approximately 7 days of cpu time on a parallel Blue-Gene machine with 128 processors. At the moment, this is the smallest frequency we can simulate so as to obtain reliable results.

As with the simulations for homogeneous slip boundary conditions, we carried out simulations at frequencies of $2\pi/100$, $2\pi/40, 2\pi/30, 2\pi/20$, and $2\pi/10$ rads/τ keeping the pattern length constant at $kw=\pi/2$. The resulting transverse velocity profile for the case $\omega=2\pi/10$ rads/τ is shown in Fig. 14. Since we have taken these averages after every $T\tau$ time the velocity profile has a similar form to the constant body force case. To compare the magnitude of the transverse velocity with the constant body force case we have calculated the transverse velocity profile for the same setup with the constant body force ($F_0=0.05$) by taking 5000 averages (see Fig. 15). The transverse velocity profile in Fig. 14 is shifted compared to the constant body force case in Fig. 15. This result also complements the viscoelasticity of the fluid. With oscillatory body force, the maximum value of the transverse velocity has increased to 0.0288 (compared to a maximum value of 0.0236 in the constant body force case). This represents a 22% increase in the transverse velocity. Results of simulations for other values of ω are given in Table I. In general, we find the increase is on average 20%, compared to a constant body force, and given we have applied a maximum 10% increase in the body force this represents a reasonable increase. We see that the maximum transverse velocity does not change appreciably with increasing frequency. Thus although our simulations agrees with the continuum theory in that a sinusoidally varying body force will increase the transverse velocity, the simulations do not show transverse velocities which increase as ω increases. We believe the reason for this is that the simplified continuum model includes only a single Λ while the fluid modeled is characterized by several relaxation constants. Instead the transverse velocity be a function of a superposition of velocities corresponding each relaxation constant. Hence Eq. (26) does not hold.

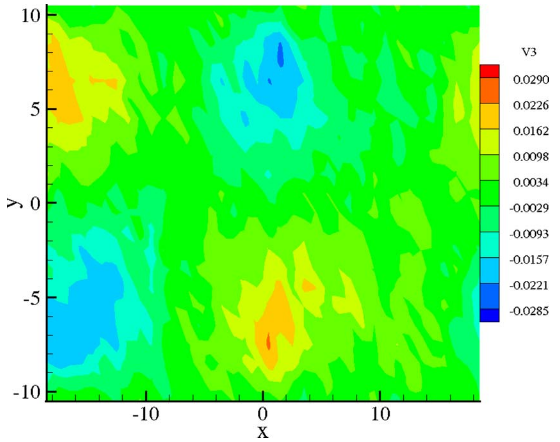

FIG. 14. (Color online) Transverse velocity profile $u_y(x,y)$ for the time dependent body force case for the frequency $\omega=2\pi/10$.

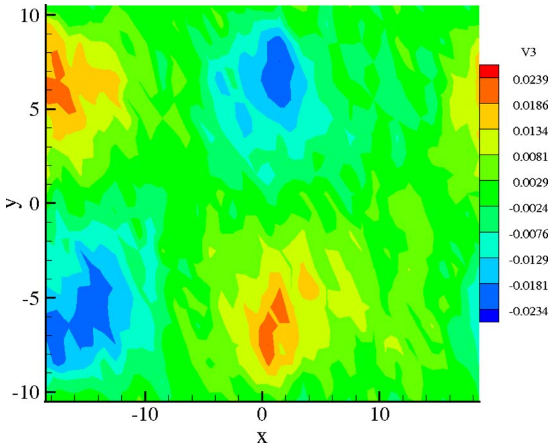

FIG. 15. (Color online) Transverse velocity profile $u_y(x,y)$ for constant body force case with 5000 averages.

Another deficiency of the continuum model [19] is that it is only a linear viscoelastic model. When compared to our MD simulations this is not such a serious problem, since we use perturbations, ϵ which are quite small (i.e., 10% of mean body force). However, certainly for larger perturbations a nonlinear model would be more appropriate.

V. SUMMARY

In this study we have sort to model the flow of polymeric fluids in narrow channels at a microscopic level. We have focused on enhancing the mixing in these fluids with a combination of active and passive techniques. The passive method is to pattern the channel boundaries with regions of high and low slip while the active method is to employ a sinusoidally varying pressure. We first modeled the passive method by varying the interaction between monomers and wall atoms. The polymeric fluid was characterized as a shear thinning fluid and we found significant transverse flows especially when the pattern spacing was greater than the radius of gyration of a polymer chain. In this case polymers can tend to stick or slip adjacent to the different patterned regions and thus perturb the dominant Poiseuille flow. In the case that the pattern spacing is smaller than the radius of gyration of the polymer chains the transverse velocity is suppressed, since now the polymer chains span two or more regions and begin to interact with them as if the boundaries are homogeneous. Thus the flow returns to being strongly Poiseuille-like. Snapshots of individual polymer chains reveal that they take up more closely bound conformations in contrast to other studies [15] where the polymer chains were found to stretch in the direction of the flow. We attribute this difference to the patterning on the walls which causes the chains to respond differently depending on the region they are adjacent to. In general we found qualitative agreement with previous continuum theory [19]. We made quantitative comparison with this theory and have found good agreement on the magnitude of the generated transverse velocity.

We proceeded to consider the effect of an offset arrangement of the patterned regions. In this case, although the magnitude of the transverse velocity did not increase it was an improvement on the previous case, since now transverse flow is generated throughout the width of the channel (see Fig. 11). In the case where the patterned regions are aligned on either side of the channel, transverse flow is zero in the middle of the channel for the entire length of the channel. Hence fluid in this region will not mix due to fluid convection (only via diffusion).

We have continued on to couple a sinusoidally varying pressure gradient with the patterned boundary conditions. In this case the continuum theory had predicted an enhancement of the transverse velocity. Our simulations also found an enhancement of the transverse flow for a sinusoidally varying pressure. The increase was reasonable—a 20% increase corresponding to a 10% increase in the amplitude of the pressure. The continuum modeling however predicted that this transverse velocity should increase with frequency. Our simulations did not show this for two reasons: (i) the polymeric fluid was found to have a number of relaxation constants (whereas the continuum theory only assumed one) and (ii) there is an upper bound on the magnitude of frequency, since polymer chains cannot respond sufficiently quickly for large frequencies.

Finally, it would be interesting to consider the effects of regions of zero shear stress (infinite slip) as studied for simple fluids by molecular dynamics by Cottine-Bionne *et al.* [10] and experimentally by Ou *et al.* [18]. However, such a situation is difficult theoretically using the perturbative approach tested here. Nonetheless, this will be addressed in future work. We note that the device in Ref. [18] based on the principal of alternating no slip and zero shear stress regions enhanced mixing by almost an order of magnitude. Based on our results here, we would expect that similar efficiencies could be achieved provided the patterning length scales are greater than the radius of gyration of the polymer.

ACKNOWLEDGMENTS

All simulations were carried out using the LAMMPS molecular dynamics package. We are also thankful to the supercomputing facilities at The University of Canterbury, New Zealand.

[1] N. T. Nguyen and Z. Wu, J. Micromech. Microeng. **15**, R1 (2005).
[2] J. M. Ottino and S. Wiggins, Philos. Trans. R. Soc. London, Ser. A **362**, 923 (2004).
[3] D. J. Beebe, G. A. Mensing, and G. M. Walker, Annu. Rev. Biomed. Eng. **4**, 261 (2002).
[4] C. H. Choi, K. Johan, A. Westin, and K. S. Breuer, Phys. Fluids **15**, 2897 (2003).
[5] D. Byun, J. Kim, H. S. Ko, and H. C. Park, Phys. Fluids **20**, 113601 (2008).
[6] S. Granick, Y. Zhu, and H. Lee, Nature Mater. **2**, 221 (2003).
[7] P. A. Thompson and S. M. Troian, Nature (London) **389**, 360 (1997).
[8] Y. Zhu and S. Granick, Phys. Rev. Lett. **88**, 106102 (2002).
[9] R. Pit, H. Hervet, and L. Léger, Phys. Rev. Lett. **85**, 980 (2000).
[10] C. Cottin-Bionne, J.-L. Barrat, L. Bocquet, and E. Charlaix, Nature Mater. **2**, 237 (2003).
[11] E. Lauga and H. A. Stone, J. Fluid Mech. **489**, 55 (2003).
[12] J.-L. Barrat and L. Bocquet, Phys. Rev. Lett. **82**, 4671 (1999).
[13] G. Nagayama and P. Cheng, Int. J. Heat Mass Transfer **47**, 501 (2004).
[14] Y. Zhu and S. Granick, Phys. Rev. Lett. **87**, 096105 (2001).
[15] R. Khare, J. J. de Pablo, and A. Yethiraj, Macromolecules **29**, 7910 (1996).
[16] O. Kuksenok, J. M. Yeomans, and A. C. Balazs, Phys. Rev. E **65**, 031502 (2002).
[17] S. C. Hendy, M. Jasperse, and J. Burnell, Phys. Rev. E **72**, 016303 (2005).
[18] J. Ou, G. R. Moss, and J. P. Rothstein, Phys. Rev. E **76**, 016304 (2007).
[19] G. G. Pereira, J. Non-Newtonian Fluid Mech. **157**, 197 (2009).
[20] G. S. Grest and K. Kremer, Phys. Rev. A **33**, 3628 (1986).
[21] P. A. Thompson and M. O. Robbins, Phys. Rev. A **41**, 6830 (1990).
[22] M. P. Allen and D. J. Tildesley, *Computer Simulation of Liquids* (Clarendon, Oxford, 1987).
[23] R. Auhl, R. Everaers, G. S. Grest, K. Kremer, and S. J. Plimpton, J. Chem. Phys. **119**, 12718 (2003).
[24] N. V. Priezjev and S. M. Troian, Phys. Rev. Lett. **92**, 018302

(2004).
[25] A. Niavarani and N. V. Priezjev, Phys. Rev. E **77**, 041606 (2008).
[26] J. H. Irving and J. G. Kirkwood, J. Chem. Phys. **18**, 817 (1950).
[27] A. Jabbarzadeh, J. D. Atkinson, and R. I. Tanner, Macromolecules **36**, 5020 (2003).
[28] R. B. Bird, R. C. Armstrong, and O. Hassager, *Dynamics of Polymeric Liquids* (John Wiley and Sons, New York, 1987), Vol. 1: Fluid Mechanics.
[29] A. Jabbarzadeh, J. D. Atkinson, and R. I. Tanner, J. Chem. Phys. **110**, 2612 (1999).
[30] T. Aoyagi and M. Doi, Comput. Theor. Polym. Sci. **10**, 317 (2000).
[31] B. D. Todd, D. J. Evans, and P. J. Daivis, Phys. Rev. E **52**, 1627 (1995).
[32] K. P. Travis, B. D. Todd, and D. J. Evans, Physica A **240**, 315 (1997).